One-phonon calculation of atom-surface inelastic scattering of the He-Cu(111) system

Yeu Wang, B. H. Choi, and N. L. Liu
Department of Physics, University of California at Riverside, Riverside, California 92521
(Received 3 August 1990; revised manuscript received 5 December 1990)

With use of the distorted-wave Born approximation derived from an *ab initio* time-independent scattering theory, an expression for the differential reflection coefficient for one-phonon transitions is presented. In addition, the relation between the truncation of the interaction potential and the Debye-Waller factor is discussed. Numerical calculations are carried out for the He-Cu(111) system. The copper surface is taken to be a slab of 80 layers with nearest-neighbor interactions for the computation of the phonon dispersion relations and polarization vectors. The plate modes corresponding to the lowest two nearly-degenerate dispersion curves are mapped onto the Rayleigh modes. With use of a pair potential proposed by others, the differential reflection coefficient for one-phonon transitions corresponding to the Rayleigh modes is calculated. The phonon wave vectors are chosen to lie along the $\langle 1\bar{1}0 \rangle$ direction, with magnitudes ranging from 0.05 to 0.60 Å^{-1}. The shape of the differential reflection coefficient is in good agreement with experiment. It is found that the projectile mainly interacts with the vibrational motion of the atoms in the first layer of the crystal and that the interactions involving the displacements of the second or deeper layers only reduce the differential reflection coefficient slightly. The change in the differential reflection coefficient due to the Debye-Waller factor is found to be small, as the temperature increases from 60 to 300 K. Further, it is found that the differential reflection coefficient increases with increasing temperature due to the Bose-Einstein distribution of the phonons and is larger for phonon annihilation than for phonon emission because of the density of the final states of the projectile and the kinematic conditions of the scattering.

I. INTRODUCTION

Scattering of thermal-energy helium atoms from a nonrigid crystal surface has been a useful technique to probe surface structure and defects.[1–4] From the conservation of energy and parallel crystal momentum derived from scattering theory, phonon spectra can be obtained by measuring the energy gain or loss and scattering angles.[5–8] Many theories of surface lattice dynamics have been developed to calculate the dispersion relations and the polarization vectors.[9–16] The surface force constants between the crystal atoms can be inferred by comparing the dispersion curves calculated from theoretical models of the lattice dynamics with those determined from experiment, especially in the region of short phonon wavelengths.[5,17–20] The intensity of the peaks provides information of the atom-surface interaction involving phonons.

Recently there have been several theoretical approaches of the scattering processes including the distorted-wave Born approximation (DWBA),[21–24] DWBA with normalization,[25] the close-coupling calculation of scattering matrix,[26,27] and the unitary one-phonon approximation.[28] In addition, a semiclassical scheme has been employed for phonon inelastic collisions,[29–31] and the optical-potential method has been developed with inclusion of phonons.[32–34] A systematic *ab initio* quantum-mechanical formulation with realistic approximation schemes was derived by Choi and Poe for phonon inelastic collisions based on a time-independent scattering theory.[35]

While various atom-surface interaction model potentials involving thermal vibrations of the crystal surface have been employed to calculate the inelastic scattering,[36–39] our present formulation is applicable to an arbitrary atom–nonrigid-surface interaction potential.[35] This flexibility allows one to understand the atom-surface interaction from a more fundamental point of view than the phenomenological approach. Further, the three-body effect can be included in a straightforward manner in our approach, if necessary.

In most other formulations the one-phonon inelastic scattering was defined in terms of the ionic displacement operator from the equilibrium position, i.e., the phonon creation or annihilation operators, in a first-order expansion of the atom-surface interaction potential. We adopt here a more physical point of view that the initial and the final phonon states of the scattering matrix element contain the same occupation numbers except in a certain mode, in which the occupation numbers differ by 1. We then say that the transition between these phonon states takes place in that mode. The expression of the differential reflection coefficient to be used in this paper contains no sum of different transition modes. In view of the flexibility of the input potential and more physical treatment of the phonon process, we employ this formulation[35] in the present calculation.

There have been discussions of the temperature dependence of the atom-surface scattering intensities involving creation or annihilation of phonons.[40,41] However, a direct atom-surface analogy of the Debye-Waller factor of neutron scattering from a bulk crystal is not available

except in some limiting cases.[42] In practice, the form of the relevant factor usually depends on the potential used. We keep the Debye-Waller factor in a general form suitable for the formulation with any pair potential, and define from this form the temperature-dependent Debye-Waller coefficients for a numerical evaluation.

In this paper we investigate one-phonon inelastic scattering of helium atoms from the copper (111) surface. We examine how the atom-surface interaction through Rayleigh modes affects the differential reflection coefficient. The differential reflection coefficient is calculated as a function of phonon wave vectors along the $\langle 1\bar{1}0\rangle$ direction. The shape of the differential reflection coefficient from our calculation is in good agreement with experiment.[43] We find the interaction of the projectile with the surface layer to be the most important quantity to consider, especially for phonon wave vectors greater than about 0.60 Å^{-1}. In addition we find that the temperature dependence of the differential reflection coefficient is mainly determined by the Bose-Einstein distribution and any changes due to the Debye-Waller factor alone are small as the temperature increases from 60 to 300 K. Also we find that the kinematic conditions of the scattering favor phonon-emission processes at high temperatures.

In Sec. II we first outline the calculation of the surface lattice dynamics. We then briefly review the transition matrix of the atom-surface inelastic scattering and derive an expression for the thermally averaged transition matrix for one-phonon transitions. The effect of the transition on the reflection coefficient calculated to the first order of the displacement of the crystal atom is also discussed. In Sec. III we present numerical calculations of the dispersion relations, the Rayleigh modes, and the Debye-Waller coefficients for a slab of 80 layers of Cu atoms. The atom–rigid-surface potential is obtained numerically from the helium–metal-atom pair potential. By specifying the kinematic conditions of the scattering, we calculate the differential reflection coefficient and analyze the interaction depth between the projectile and the vibration of the crystal atoms. The effect of the surface temperature is also examined. A summary of our calculation is presented at the end of this paper.

II. THEORY

A. Lattice dynamics of crystals with a surface

The relevant vectors defining the projectile-crystal system with the origin on the surface and the positive z axis along the outward normal to the surface are shown in Fig. 1. We assume that the crystal is of infinite extent in the x and the y directions with translational-invariance symmetry in the x-y plane. We treat the slab crystal as two dimensional, with each unit cell containing atoms distributed down through all the layers. These unit cells are referred to as surface unit cells. We assume one atom per surface unit cell in a given layer. We denote by $\mathbf{R}_G$ the two-dimensional direct-lattice vector parallel to the surface and $\mathbf{G}$ the corresponding parallel reciprocal-lattice vector generated by $\mathbf{G}$. Thus $\mathbf{R}_G = m\,\mathbf{A}_1 + n\,\mathbf{A}_2$

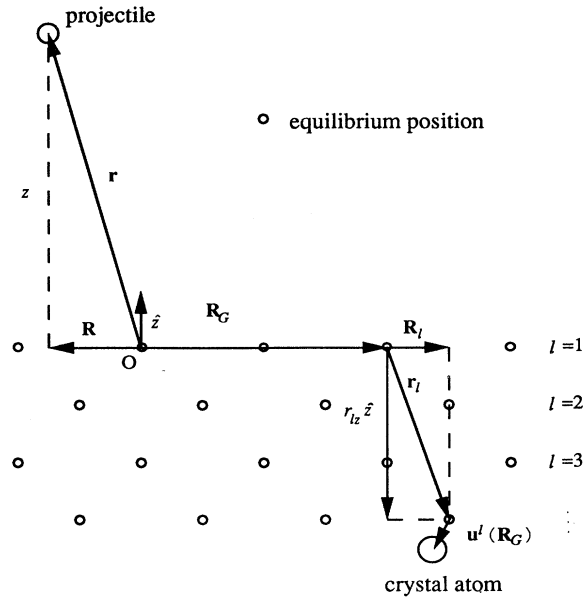

FIG. 1. The vectors defining the projectile-crystal system.

and $\mathbf{G} = m\,\mathbf{B}_1 + n\,\mathbf{B}_2$ where $\mathbf{A}_1$ and $\mathbf{A}_2$ are the primitive direct-lattice vectors and $\mathbf{B}_1$ and $\mathbf{B}_2$ are the corresponding reciprocal-lattice vectors with $\mathbf{A}_i \cdot \mathbf{B}_j = 2\pi\delta_{ij}$. When used as superscript or subscript, $\mathbf{G}$ is denoted simply by G. We choose the surface unit cells to be primitive cells and denote the equilibrium position of an atom in the lth layer of a surface unit cell corresponding to $\mathbf{R}_G$ by the vector $\mathbf{R}_G + \mathbf{r}_l$. The lth-layer equilibrium atomic configuration is obtained from that of the first layer by a translation vector $\mathbf{r}_l - \mathbf{r}_1$. The vector $\mathbf{r}_l$ is uniquely determined up to $\mathbf{R}_G$. The displacement of the atom from its equilibrium position is denoted by $\mathbf{u}^l(\mathbf{R}_G)$ which can be put in the operator form,

$$\mathbf{u}^l(\mathbf{R}_G) = \frac{1}{\sqrt{N}} \sum_{\mathbf{Q},s} \left[\frac{\hbar}{2\omega_s(\mathbf{Q})} \right]^{1/2} (a_{\mathbf{Q},s} + a^{\dagger}_{-\mathbf{Q},s}) \times \epsilon_s^l(\mathbf{Q}) e^{i\mathbf{Q}\cdot\mathbf{R}_G} , \quad (1)$$

employing normal modes with the second quantization, where $\mathbf{Q}$ is the two-dimensional phonon wave vector parallel to the surface, $\omega_s(\mathbf{Q})$ the frequency and $\epsilon_s^l(\mathbf{Q})$ the polarization vector corresponding to mode s. $\mathbf{Q}$'s lie in the first two-dimensional Brillouin zone. We impose the orthonormality condition

$$\sum_l \epsilon_s^{l*}(\mathbf{Q}) \cdot \epsilon_{s'}^l(\mathbf{Q}) M_{\text{cr}} = \delta_{ss'} , \quad (2)$$

where M_{cr} is the mass of the crystal atom. Here $a_{\mathbf{Q},s}$ is the annihilation operator for the mode $(\mathbf{Q},s)$ and its adjoint operator $a^{\dagger}_{\mathbf{Q},s}$ the creation operator. They satisfy the Boson commutation relations $[a_{\mathbf{Q},s}, a^{\dagger}_{\mathbf{Q}',s'}] = \delta_{\mathbf{Q}\mathbf{Q}'}\delta_{ss'}$, $[a_{\mathbf{Q},s}, a_{\mathbf{Q}',s'}] = [a^{\dagger}_{\mathbf{Q},s}, a^{\dagger}_{\mathbf{Q}',s'}] = 0$. We impose the two-

dimensional Born–von Kármán boundary condition with $N \equiv N_1 N_2$ being the total number of unit cells on the surface. The portion of the crystal containing the N unit cells is sometimes called the "large primitive cell" since it repeats itself along the surface of the crystal. The Hamiltonian of the harmonic crystal $H_{\rm cr}$ is expressed in terms of the displacement $\mathbf{u}^l(\mathbf{R}_G)$ and the corresponding momentum. In terms of the normal modes the crystal Hamiltonian is given by $H_{\rm cr} = \sum_{\mathbf{Q},s} \hbar\omega_s(\mathbf{Q})(a^\dagger_{\mathbf{Q},s} a_{\mathbf{Q},s} + \frac{1}{2})$ with the phonon eigenstates denoted by $|\ldots, n_{\mathbf{Q},s}, \ldots\rangle$, where $n_{\mathbf{Q},s}$ is the occupation number of mode $(\mathbf{Q},s)$. To simplify the notation we define $|n\rangle = |\ldots, n_{\mathbf{Q},s}, \ldots\rangle$. The phonon states satisfy the orthonormality relation $\langle n|n'\rangle = \delta_{nn'}$ and the completeness relation $\sum_n |n\rangle\langle n| = 1$. The energy of $|n\rangle$ is given by $\mathcal{E}_n \equiv \sum_{\mathbf{Q},s} \hbar\omega_s(\mathbf{Q})(n_{\mathbf{Q},s} + \frac{1}{2})$. The total parallel crystal momentum operator $\hbar\mathcal{K}_{\rm cr}$ is defined by $\mathcal{K}_{\rm cr} \equiv \sum_{\mathbf{Q},s} \mathbf{Q} a^\dagger_{\mathbf{Q},s} a_{\mathbf{Q},s}$ with eigenvalue $\mathbf{Q}_n = \sum_{\mathbf{Q},s} \mathbf{Q} n_{\mathbf{Q},s}$.

B. The atom-crystal surface scattering

In what follows we adopt the method of scattering dynamics and notations described in Ref. 35. The position of the atomic projectile relative to the origin will be denoted by $\mathbf{r}$, its projection on the crystal surface by $\mathbf{R}$, the initial (final) momentum of the projectile by $\mathbf{k}_i$ ($\mathbf{k}_f$), and $\mathbf{K}_i$ ($\mathbf{K}_f$) the projection. The projectile-crystal interaction potential V and the total Hamiltonian of the system H satisfy the two-dimensional translational invariance,[35]

$$U_G V U_G^\dagger = V \tag{3a}$$

and

$$U_G H U_G^\dagger = H \tag{3b}$$

for all $\mathbf{G}$, where

$$H \equiv -\frac{\hbar^2}{2M}\nabla_{\mathbf{r}}^2 + H_{\rm cr} + V \tag{4}$$

with M the mass of the projectile and

$$U_G \equiv e^{i\hbar^{-1}\mathbf{P}\cdot\mathbf{R}_G} e^{i\mathcal{K}_{\rm cr}\cdot\mathbf{R}_G} = e^{i(\mathbf{P}/\hbar + \mathcal{K}_{\rm cr})\cdot\mathbf{R}_G} \tag{5}$$

with $\mathbf{P}$ being the projection of the momentum operator of the projectile onto the surface. The time-independent Schrödinger equation of the system takes the form

$$H\psi^{(+)}(\mathbf{r}) = E\psi^{(+)}(\mathbf{r}) \tag{6}$$

where $E \equiv \hbar^2 k_i^2/(2M) + \mathcal{E}_{n_i}$ is the total energy and $\psi^{(+)}(\mathbf{r})$ is the phonon-dependent wave function of the system. From Eq. (3b) we see that $\mathbf{K} \equiv \mathbf{K}_i + \mathbf{Q}_{n_i}$ is a good quantum number up to $\mathbf{G}$. The wave function is required to satisfy the asymptotic behavior of an incident wave plus scattered waves. Using Eqs. (3a) and (3b) the wave function and the interaction potential V can be written, respectively, in the forms[35]

$$\psi^{(+)}_{\mathbf{K}}(\mathbf{r}) \equiv \psi^{(+)}(\mathbf{r}) = \sum_{n,\mathbf{G}} \psi^{(+)}_{nG}(z)|n\rangle e^{i(\mathbf{K}-\mathbf{Q}_n+\mathbf{G})\cdot\mathbf{R}}, \tag{7a}$$

$$V = \sum_{n,n',\mathbf{G}} |n\rangle V^G_{n,n'}(z)\langle n'| e^{i(\mathbf{Q}_{n'}-\mathbf{Q}_n+\mathbf{G})\cdot\mathbf{R}}, \tag{7b}$$

where each term in the sum of Eq. (7a) is referred to as a channel, which we will denote by $(n,\mathbf{G})$. If V becomes large compared with the vertical kinetic energy of the projectile as it approaches the surface, then $\psi^{(+)}_{nG}(z)$ decays rapidly to zero. We approximate this requirement by the boundary condition that $\psi^{(+)}_{nG}(z_0) = 0$ where z_0 is the point below which the wave functions are essentially zero. Substituting Eqs. (7a) and (7b) into the Schrödinger equation (6) we get a close-coupling equation for $\psi^{(+)}_{nG}(z)$ involving the potential matrix $V^G_{n,n'}(z)$. The asymptotic behavior of the incident plus scattered wave then becomes[35]

$$\psi^{(+)}_{nG,n_i0}(z) \sim \begin{cases} \left[\dfrac{k_{n_i0}}{k_{nG}}\right]^{1/2} (e^{-ik_{nG}z}\delta_{G0}\delta_{nn_i} - S^{(+)}_{nG,n_i0} e^{ik_{nG}z}) & \text{(open channel)}, \\ -\left[\dfrac{k_{n_i0}}{\kappa_{nG}}\right]^{1/2} \bar{S}^{(+)}_{nG,n_i0} e^{-\kappa_{nG}z} & \text{(closed channel)}, \end{cases} \tag{8}$$

as z goes to infinity, where

$$k^2_{nG} \equiv \frac{2M}{\hbar^2}(E - \mathcal{E}_n) - (\mathbf{K} - \mathbf{Q}_n + \mathbf{G})^2 . \tag{9}$$

If $k^2_{nG} < 0$, we write $k^2_{nG} = -\kappa^2_{nG}$ with $\kappa_{nG} > 0$.

The coupled differential equations are difficult to solve numerically and we introduce an approximation based on the two-potential formalism. We write $V = v_0(z) + \tilde{V}$ where $\tilde{V} \equiv V - v_0(z)$ and is expected to be small compared with $v_0(z)$. In our calculation $v_0(z)$ is chosen to be the laterally averaged potential (see Sec. III C)

$$v_0(z) \equiv \frac{1}{S}\int_{\rm u.c.} \left[\sum_{G,l} u(|\mathbf{r} - \mathbf{R}_G - \mathbf{r}_l|)\right] d^2R , \tag{10}$$

where the integration is over the unit cell (u.c.). For each channel we consider the wave function distorted by $v_0(z)$

$$\chi^{0(+)}_{\mathbf{K},nG}(\mathbf{r}) \equiv \chi^{0(+)}_{nG}(z)|n\rangle e^{i(\mathbf{K}-\mathbf{Q}_n+\mathbf{G})\cdot\mathbf{R}} \tag{11}$$

which satisfies the unperturbed Schrödinger equation

$$\left[-\frac{\hbar^2}{2M}\nabla_{\mathbf{r}}^2 + H_{\rm cr} + v_0(z)\right]\chi^{0(+)}_{\mathbf{K},nG}(\mathbf{r}) = E\chi^{0(+)}_{\mathbf{K},nG}(\mathbf{r}) \tag{12}$$

with the boundary condition $\chi_{nG}^{0(+)}(z_0)=0$. Then $\chi_{nG}^{0(+)}(z)$ has the asymptotic behaviors

$$\chi_{nG}^{0(+)}(z)\sim\begin{cases} e^{-ik_{nG}z}-s_{nG}^{(+)}e^{ik_{nG}z} & \text{(open channel)} \\ e^{\kappa_{nG}z}-\bar{s}_{nG}^{(+)}e^{-\kappa_{nG}z} & \text{(closed channel)}, \end{cases} \tag{13}$$

where $s_{nG}^{(+)}=e^{2i\delta_{nG}}$ with δ_{nG} being the phase shift from the potential $v_0(z)$. Also we define the wave function

$$\chi_{\mathbf{K},nG}^{0(-)}(\mathbf{r})\equiv\chi_{nG}^{0(-)}(z)|n\rangle e^{i(\mathbf{K}-\mathbf{Q}_n+\mathbf{G})\cdot\mathbf{R}}$$

with $\chi_{nG}^{0(-)}(z)\equiv\chi_{nG}^{0(+)*}(z)$ so that it satisfies Eq. (12) and has the asymptotic behavior with incoming scattered waves. For the channel $(n_i,\mathbf{0})$ we have $k_{n_i0}=-k_{iz}>0$ and for $(n_f,\mathbf{G}_f)$ we have $k_{n_fG_f}^2=k_{fz}^2$ from the conservation of the parallel crystal momentum. For the open channel we choose $k_{fz}>0$ so that $k_{n_fG_f}=k_{fz}$. The close-coupling equations mentioned before can be transformed to an integral equation. Combining the asymptotic behavior given by Eq. (8) and the integral equation, we have the following expression of the scattering matrix:

$$S_{n_fG_f,n_i0}^{(+)}=\delta_{n_fn_i}\delta_{G_f0}s_{n_fG_f}^{(+)}+\frac{iM}{\hbar^2(k_{n_fG_f}k_{n_i0})^{1/2}L^2}\int d\mathbf{r}\,\chi_{\mathbf{K},n_fG_f}^{0(-)}(\mathbf{r})\tilde{V}(\mathbf{r})\psi_{\mathbf{K},n_i0}^{(+)}(\mathbf{r})\ . \tag{14}$$

The transition matrix is defined by

$$T_{n_fG_f,n_i0}\equiv\frac{\hbar^2(k_{n_fG_f}k_{n_i0})^{1/2}}{iML}S_{n_fG_f,n_i0}^{(+)}\ . \tag{15}$$

In the distorted-wave Born approximation (DWBA), we set

$$\psi_{\mathbf{K},n_i0}^{(+)}(\mathbf{r})\approx\chi_{\mathbf{K},n_i0}^{(+)}(\mathbf{r}) \tag{16}$$

and therefore

$$T_{n_fG_f,n_i0}=\frac{1}{L^3}\int_{z_0}^{\infty}dz\,\chi_{n_fG_f}^{0(-)*}(z)\tilde{V}_{n_f,n_i}^{G_f}(z)\chi_{n_i0}^{0(+)}(z)\ , \tag{17}$$

where

$$\tilde{V}_{n,n'}^{G,G'}(z)\equiv V_{n,n'}^{G,G'}(z)-v_0(z)\delta_{nn'}\delta_{GG'} \tag{18}$$

for $n_f\neq n_i$. The initial and the final states are open channels.

C. Application to one-phonon transition

The q-phonon transition between the initial and the final phonon state $|n_i\rangle$ and $|n_f\rangle$ is in general defined such that their occupation numbers $n_{i_{\mathbf{Q}',s'}}$ and $n_{f_{\mathbf{Q}',s'}}$ satisfy

$$\sum_{\mathbf{Q}',s'}|n_{f_{\mathbf{Q}',s'}}-n_{i_{\mathbf{Q}',s'}}|=q\ . \tag{19}$$

This includes any changes of the occupation numbers in every mode $(\mathbf{Q}',s')$ of $|n_i\rangle$ and $|n_f\rangle$. We consider one-phonon transitions in mode $(\mathbf{Q},s)$ between $|n_i\rangle$ and $|n_f\rangle$. Then from Eq. (19) with $q=1$

$$n_{f_{\mathbf{Q}',s'}}-n_{i_{\mathbf{Q}',s'}}=\pm\delta_{\mathbf{Q}\mathbf{Q}'}\delta_{ss'}\ . \tag{20}$$

We use the upper sign to denote phonon emission and the lower sign phonon annihilation. In our formulation only the initial and the final states are physically observable. We include only transitions defined in the above so that for either phonon emission or annihilation the final phonon state is uniquely determined, once the initial phonon state is specified. The differntial reflection coefficient is defined by

$$\dot{I}=\rho_i v_i\frac{dR}{d\Omega_f}d\Omega_f\ , \tag{21}$$

where $\dot{I}$ is the number of particles entering the detector per unit time, ρ_i is the number density of the incident beam, v_i is the speed of the incident particles, and $d\Omega_f$ the differential solid angle in the direction of the detector. For projectiles satisfying the momentum conservation

$$\mathbf{K}_f-\mathbf{K}_i=\mp\mathbf{Q}+\mathbf{G}_f \tag{22a}$$

and the energy conservation

$$E_f^P-E_i^P=\mp\hbar\omega_s(\mathbf{Q})\ , \tag{22b}$$

the thermally averaged differential reflection coefficient for the one-phonon transition can be written as

$$\frac{dR}{d\Omega_f}=\left[\frac{ML^2}{2\pi\hbar^2}\right]^2\frac{k_f}{|k_{iz}|}\frac{\langle|T_{n_fG_f,n_i0}|^2\rangle_T}{|1-(\hbar/2E_f^P)\nabla_{\mathbf{Q}}\omega_s(\mathbf{Q})\cdot\mathbf{K}_f|}\ , \tag{23}$$

where the angled brackets denote the thermal average over the initial phonon states. There is no sum over the final phonon states in the above equation.

D. The thermally averaged transition matrix

We denote by $u(\mathbf{r})$ the pairwise representation of the interaction potential between the atomic projectile and the atoms of the crystal. Assuming the sum of this pairwise form of interaction over the atoms in the crystal provides an adequate description of the realistic system, we can write the interaction potential between the projectile and the surface as

$$V=V(\mathbf{r},\mathbf{u}^l(\mathbf{R}_G))=\sum_{G,l}u[\mathbf{r}-\mathbf{R}_G-\mathbf{r}_l-\mathbf{u}^l(\mathbf{R}_G)]\ . \tag{24}$$

To carry out numerical calculation we outline the steps and the approximations used to obtain $\langle|T_{n_fG_f,n_i0}|\rangle_T$ for the one-phonon transition. We expand $u(\mathbf{r})$ in the Fourier series

$$u(\mathbf{r})=\frac{1}{L^3}\sum_{\mathbf{k}}u_{\mathbf{k}}e^{i\mathbf{k}\cdot\mathbf{r}}\ . \tag{25}$$

Taking into account Eqs. (24) and (1) we have

$$V^{G}_{n,n'}(z)=\frac{1}{L^3}\sum_{G',l,k_z} u_{\mathbf{k}_G}\exp\{i[k_z z+(\mathbf{Q}_n-\mathbf{Q}_{n'})\cdot\mathbf{R}_{G'}-\mathbf{k}_G\cdot\mathbf{r}_l]\}\left\langle n\left|\exp\sum_{\mathbf{Q},s}(-\alpha a^{\dagger}_{\mathbf{Q},s}+\alpha^* a_{\mathbf{Q},s})\right|n'\right\rangle \tag{26}$$

where $\mathbf{k}_G\equiv k_z\hat{\mathbf{z}}+\mathbf{G}+\mathbf{Q}_{n'}-\mathbf{Q}_n$ and

$$\alpha\equiv i\left[\frac{\hbar}{2N\omega_s(\mathbf{Q})}\right]^{1/2}\mathbf{k}_G\cdot\boldsymbol{\epsilon}^{l*}_s(\mathbf{Q})e^{-i\mathbf{Q}\cdot\mathbf{R}_{G'}}\ . \tag{27}$$

For convenience we denote the mode $(\mathbf{Q},s)$ by ξ. Using the Baker-Hausdorff identity $e^{A+B}=e^{A}e^{B}e^{-\frac{1}{2}[A,B]}$, we have

$$\langle n_\xi|e^{-\alpha a^{\dagger}_\xi+\alpha^* a_\xi}|n'_\xi\rangle=e^{-|\alpha|^2/2}\sum_{i,j=0}^{\infty}\frac{(-\alpha)^i(\alpha^*)^j}{i!\,j!}\langle n_\xi|(a^{\dagger}_\xi)^i(a_\xi)^j|n'_\xi\rangle\ . \tag{28}$$

Therefore, the potential matrix element can be written as

$$V^{G}_{n,n'}(z)=\frac{N}{L^3}\sum_{l,k_z}u_{\mathbf{k}_G}e^{i(k_z z-\mathbf{k}_G\cdot\mathbf{r}_l)}\prod_\xi\left[\gamma^{|n_\xi-n'_\xi|}\left[\frac{\max(n_\xi,n'_\xi)!}{\min(n_\xi,n'_\xi)!}\right]^{1/2}\right]$$
$$\times\prod_\xi\left[e^{-|\alpha|^2/2}\sum_{j=0}^{\min(n_\xi,n'_\xi)}\frac{\min(n_\xi,n'_\xi)!}{j![\min(n_\xi,n'_\xi)-j]!}\frac{(-1)^j|\alpha|^{2j}}{(|n_\xi-n'_\xi|+j)!}\right], \tag{29}$$

where

$$\gamma\equiv -i\left[\frac{\hbar}{2N\omega_s(\mathbf{Q})}\right]^{1/2}\mathbf{k}_G\cdot\begin{cases}\boldsymbol{\epsilon}^{l*}_s(\mathbf{Q}), & n_\xi\geq n'_\xi\\ \boldsymbol{\epsilon}^{l}_s(\mathbf{Q}), & n_\xi<n'_\xi\end{cases}. \tag{30}$$

The products are taken over all modes in the first Brillouin zone. For one-phonon transition we need only $V^{G_f}_{n_f,n_i}(z)$ with Eq. (20) satisfied. Then $\mathbf{Q}_{n_f}-\mathbf{Q}_{n_i}=\mp\mathbf{Q}$ which is limited to the length of the first Brillouin zone at most. If G_f is large, then $u_{\mathbf{k}_{G_f}}$ and thus $V^{G_f}_{n_f,n_i}(z)$ will be small. We consider scattering which does not involve large G_f. In addition, if $\omega_s(\mathbf{Q})$ is not close to zero and $u_{\mathbf{k}_{G_f}}$ decreases fast enough to allow early truncation of the sum over k_z, then $|\alpha|^2$ is of the order of $1/N\ll 1$. Moreover, if the average occupation numbers $\langle n_\xi\rangle_T$ are not large at the temperatures considered we approximate $1+x+\cdots$ by e^x for $|x|\ll 1$ in the sum over j in Eq. (29) for small $|\alpha|^2$. Then for one-phonon emission between $|n_i\rangle$ and $|n_f\rangle$ we obtain

$$V^{G_f}_{n_f,n_i}(z)=-\frac{i}{L^3}\left[\frac{\hbar N(n_{i\mathbf{Q},s}+1)}{2\omega_s(\mathbf{Q})}\right]^{1/2}\sum_{l,k_z}\mathbf{k}_{G_f}\cdot\boldsymbol{\epsilon}^{l*}_s(\mathbf{Q})u_{\mathbf{k}_{G_f}}e^{i(k_z z-\mathbf{k}_{G_f}\cdot\mathbf{r}_l)}e^{-W_l(\mathbf{k}_{G_f})}\ , \tag{31}$$

where

$$W_l(\mathbf{k}_{G_f})\equiv\frac{1}{2N}\sum_{\mathbf{Q},s}\frac{(n_{i\mathbf{Q},s}+\frac{1}{2})\hbar}{\omega_s(\mathbf{Q})}|\mathbf{k}_{G_f}\cdot\boldsymbol{\epsilon}^{l*}_s(\mathbf{Q})|^2 \tag{32}$$

with $\mathbf{k}_{G_f}=k_z\hat{\mathbf{z}}+\mathbf{G}_f-\mathbf{Q}=k_z\hat{\mathbf{z}}+\mathbf{K}_f-\mathbf{K}_i$. As one can see $W_l(\mathbf{k}_{G_f})$ depends on the phonon state $|n_{i\mathbf{Q},s}\rangle$. For each l in Eq. (31) the factor $\exp(n_{i\mathbf{Q}s}|\alpha|^2/2)$ with α corresponding to the transition mode $(\mathbf{Q},s)$ has been approximated by unity due to the smallness of $|\alpha|^2$. The potential matrix element for one-phonon annihilation can be obtained simply by changing $n_{i\mathbf{Q},s}+1$ to $n_{i\mathbf{Q},s}$ and $\boldsymbol{\epsilon}^{l*}_s(\mathbf{Q})$ to $\boldsymbol{\epsilon}^{l}_s(\mathbf{Q})$ with $\mathbf{k}_{G_f}=k_z\hat{\mathbf{z}}+\mathbf{G}_f+\mathbf{Q}$ where $\mathbf{G}_f=\mathbf{K}_f-\mathbf{K}_i-\mathbf{Q}$. The factor $\exp[(n_{i\mathbf{Q}s}+1)|\alpha|^2/2]$ is taken to be unity.

Assuming $\beta\hbar\omega_s(\mathbf{Q})\gg|\alpha|^2$ ($\beta\equiv 1/k_B T$ where k_B is the Boltzmann constant) one can show that

$$\langle(n_{i\mathbf{Q},s}+1)e^{-W_{l'}(\mathbf{k}'_{G_f})}e^{-W_l(\mathbf{k}_{G_f})}\rangle_T\approx(\langle n_{i\mathbf{Q},s}\rangle_T+1)e^{-\langle W_{l'}(\mathbf{k}'_{G_f})\rangle_T}e^{-\langle W_l(\mathbf{k}_{G_f})\rangle_T}\ . \tag{33}$$

By substituting the potential matrix element Eq. (31) into Eq. (17) and noting that the wave function and $\mathbf{k}_{G_f}$ are independent of the phonon occupation numbers, the thermally averaged transition matrix element can be written as

$$\langle|T_{n_f G_f,n_i 0}|^2\rangle_T=\frac{N\hbar}{4\pi^2L^6}\frac{(\langle n_{i\mathbf{Q},s}\rangle_T+1)}{2\omega_s(\mathbf{Q})}\left|\int_{z_0}^{\infty}dz\,\chi^{0(-)*}_{n_f G_f}(z)\chi^{0(+)}_{n_i 0}(z)\right.$$
$$\left.\times\int_{-\infty}^{\infty}dk_z\sum_l\mathbf{k}_{G_f}\cdot\boldsymbol{\epsilon}^{l*}_s(\mathbf{Q})u_{\mathbf{k}_{G_f}}e^{i(k_z z-\mathbf{k}_{G_f}\cdot\mathbf{r}_l)}e^{-\langle W_l(\mathbf{k}_{G_f})\rangle_T}\right|^2, \tag{34}$$

where we have made the substitution $\sum_{k_z} \rightarrow (L/2\pi)\int_{-\infty}^{\infty} dk_z$, and

$$\langle n_{i\mathbf{Q},s}\rangle_T = \frac{1}{e^{\beta\hbar\omega_s(\mathbf{Q})}-1} \tag{35}$$

is the Bose-Einstein distribution for the mode $(\mathbf{Q},s)$. The exponential factor

$$\exp[-\langle W_l(\mathbf{k}_{G_f})\rangle_T] = \exp[-i\langle \mathbf{k}_{G_f}\cdot\boldsymbol{\epsilon}_s^l(\mathbf{Q})\rangle_T] = \exp\{-\tfrac{1}{2}\langle[\mathbf{k}_{G_f}\cdot\boldsymbol{\epsilon}_s^l(\mathbf{Q})]^2\rangle_T\} \tag{36}$$

can be interpreted as the square root of the Debye-Waller factor of the system for one-phonon transitions *containing* the integration variable k_z. We write in the form of a second-order polynomial in k_z

$$\langle W_l(\mathbf{k}_{G_f})\rangle_T = A^l(T)k_z^2 + [B_1^l(T)\Delta K_x + B_2^l(T)\Delta K_y]k_z + C_1^l(T)(\Delta K_x)^2 + C_2^l(T)\Delta K_x\,\Delta K_y + C_3^l(T)(\Delta K_y)^2 , \tag{37}$$

where $\Delta\mathbf{K}\equiv\mathbf{K}_f-\mathbf{K}_i$ and

$$\begin{aligned}
A^l(T) &\equiv \frac{\hbar}{2N}\sum_{\mathbf{Q},s}\frac{\langle n_{\mathbf{Q},s}\rangle_T+\frac{1}{2}}{\omega_s(\mathbf{Q})}|\epsilon_{sz}^l(\mathbf{Q})|^2 ,\\
B_1^l(T) &\equiv \frac{\hbar}{N}\sum_{\mathbf{Q},s}\frac{\langle n_{\mathbf{Q},s}\rangle_T+\frac{1}{2}}{\omega_s(\mathbf{Q})}\{\mathrm{Re}[\epsilon_{sz}^l(\mathbf{Q})]\mathrm{Re}[\epsilon_{sx}^l(\mathbf{Q})]+\mathrm{Im}[\epsilon_{sz}^l(\mathbf{Q})]\mathrm{Im}[\epsilon_{sx}^l(\mathbf{Q})]\} ,\\
B_2^l(T) &\equiv \frac{\hbar}{N}\sum_{\mathbf{Q},s}\frac{\langle n_{\mathbf{Q},s}\rangle_T+\frac{1}{2}}{\omega_s(\mathbf{Q})}\{\mathrm{Re}[\epsilon_{sz}^l(\mathbf{Q})]\mathrm{Re}[\epsilon_{sy}^l(\mathbf{Q})]+\mathrm{Im}[\epsilon_{sz}^l(\mathbf{Q})]\mathrm{Im}[\epsilon_{sy}^l(\mathbf{Q})]\} ,\\
C_1^l(T) &\equiv \frac{\hbar}{2N}\sum_{\mathbf{Q},s}\frac{\langle n_{\mathbf{Q},s}\rangle_T+\frac{1}{2}}{\omega_s(\mathbf{Q})}|\epsilon_{sx}^l(\mathbf{Q})|^2 ,\\
C_2^l(T) &\equiv \frac{\hbar}{N}\sum_{\mathbf{Q},s}\frac{\langle n_{\mathbf{Q},s}\rangle_T+\frac{1}{2}}{\omega_s(\mathbf{Q})}\{\mathrm{Re}[\epsilon_{sx}^l(\mathbf{Q})]\mathrm{Re}[\epsilon_{sy}^l(\mathbf{Q})]+\mathrm{Im}[\epsilon_{sx}^l(\mathbf{Q})]\mathrm{Im}[\epsilon_{sy}^l(\mathbf{Q})]\} ,\\
C_3^l(T) &\equiv \frac{\hbar}{2N}\sum_{\mathbf{Q},s}\frac{\langle n_{\mathbf{Q},s}\rangle_T+\frac{1}{2}}{\omega_s(\mathbf{Q})}|\epsilon_{sy}^l(\mathbf{Q})|^2 .
\end{aligned} \tag{38}$$

We will refer to these temperature-dependent coefficients as the Debye-Waller coefficients. Then the integration over k_z in Eq. (34) can be done analytically and the thermally averaged one-phonon-emission T-matrix element between states satisfying conservation of parallel crystal momentum can be written as

$$\langle|T_{n_fG_f,n_i0}|^2\rangle_T = \frac{N\hbar}{8\pi^2L^6}\frac{\langle n_{i\mathbf{Q},s}\rangle_T+1}{\omega_s(\mathbf{Q})}A , \tag{39}$$

with

$$\begin{aligned}
A \equiv \Bigg|\sum_l e^{-i\Delta\mathbf{K}\cdot\mathbf{r}_l}&\exp[-C_1^l(T)(\Delta K_x)^2 - C_2^l(T)\Delta K_x\,\Delta K_y - C_3^l(T)(\Delta K_y)^2]\\
&\times\exp\left[\frac{[B_1^l(T)\Delta K_x + B_2^l(T)\Delta K_y]^2}{4A^l(T)}\right]\left[\frac{\pi}{A^l(T)}\right]^{1/2}\\
&\times\int_{z_0}^{\infty}dz\,\chi_{n_fG_f}^{0(-)*}(z)\chi_{n_i0}^{0(+)}(z)\int_{-\infty}^{\infty}dz'\exp\left[-\frac{(z-r_{lz}-z')^2}{4A^l(T)}\right]\\
&\qquad\times\exp\left[-i\frac{B_1^l(T)\Delta K_x + B_2^l(T)\Delta K_y}{2A^l(T)}(z-r_{lz}-z')\right]u_{\Delta\mathbf{K}}(z')\\
&\qquad\times\left[[-B_1^l(T)\Delta K_x - B_2^l(T)\Delta K_y + i(z-r_{lz}-z')]\frac{\epsilon_{sz}^{l*}(\mathbf{Q})}{2A^l(T)} + \Delta\mathbf{K}\cdot\boldsymbol{\epsilon}_s^{l*}(\mathbf{Q})\right]\Bigg|^2 ,
\end{aligned} \tag{40}$$

where $u_{\Delta\mathbf{K}}(z)$ is the two-dimensional Fourier transform of $u(\mathbf{r})=u(\mathbf{R},z)$,

$$u_{\Delta\mathbf{K}}(z) \equiv \int_{\text{whole surface}} u(\mathbf{R},z)e^{-i\Delta\mathbf{K}\cdot\mathbf{R}}\,d^2R . \tag{41}$$

We see that $\langle n_{iQ,s}\rangle_T$ is not the only temperature-dependent factor in the T-matrix element. For one-phonon annihilation, the T-matrix element is obtained by replacing $\langle n_{iQ,s}\rangle_T+1$ by $\langle n_{iQ,s}\rangle_T$ and $\epsilon_s^{l*}(\mathbf{Q})$ by $\epsilon_s^l(\mathbf{Q})$.

E. Comment on the one-phonon transition

In the case of a three-dimensional bulk crystal the one-phonon transition has been studied by truncating the interaction potential between the incident particle and the atoms in the crystal to the first order of the displacement vectors. We consider similar truncation in our atom-surface case. The term $u[\mathbf{r}-\mathbf{R}_G-\mathbf{r}_l-\mathbf{u}^l(\mathbf{R}_G)]$ in Eq. (24) can be expanded in a series of $\mathbf{u}^l(\mathbf{R}_G)$. If the temperature is not too high we need only to keep up to the first-order term of $\mathbf{u}^l(\mathbf{R}_G)$. This is equivalent to expanding the exponentials in the Fourier series Eq. (25) and keeping only up to the first-order term of $\mathbf{u}^l(\mathbf{R}_G)$. Using the V truncated at the first order of $\mathbf{u}^l(\mathbf{R}_G)$ the potential matrix element $V^G_{n,n'}(z)$ becomes the same as in Eq. (26) except that the factor $\langle n|\exp[\sum_{\mathbf{Q},s}(-\alpha a^\dagger_{\mathbf{Q},s}+\alpha^* a_{-\mathbf{Q},s})]|n'\rangle$ is replaced by

$$-i\mathbf{k}_G\cdot\langle n|\mathbf{u}^l(\mathbf{R}_{G'})|n'\rangle=-\frac{i\mathbf{k}_G}{\sqrt{N}}\cdot\sum_{\mathbf{Q},s}\left[\frac{\hbar}{2\omega_s(\mathbf{Q})}\right]^{1/2}[\langle n|a_{\mathbf{Q},s}|n'\rangle\epsilon_s^l(\mathbf{Q})e^{i\mathbf{Q}\cdot\mathbf{R}_{G'}}+\langle n|a^\dagger_{\mathbf{Q},s}|n'\rangle\epsilon_s^{l*}(\mathbf{Q})e^{-i\mathbf{Q}\cdot\mathbf{R}_{G'}}]\ . \tag{42}$$

The matrix element $\langle n|a_{\mathbf{Q},s}|n'\rangle$ can be nonzero only if n and n' satisfy $n_{Q',s'}-n'_{Q',s'}=-\delta_{QQ'}\delta_{ss'}$ for a particular mode $(\mathbf{Q},s)$. Similarly $\langle n|a^\dagger_{\mathbf{Q},s}|n'\rangle$ can be nonzero only if $n_{Q',s'}-n'_{Q',s'}=\delta_{QQ'}\delta_{ss'}$ for a particular $(\mathbf{Q},s)$. In either case this is the only nonzero term in the sum over $(\mathbf{Q},s)$. Setting $n=n_f$, $n'=n_i$, and $\mathbf{G}=\mathbf{G}_f$, we see that the potential matrix element $V^{G_f}_{n_f,n_i}(z)$ can be nonzero only if $|n_f\rangle$ and $|n_i\rangle$ satisfy the one-phonon transition Eq. (20). If there were no higher-order terms of $\mathbf{u}^l(\mathbf{R}_G)$ other than the first, then there could be no multiphonon processes. However, the reverse is not true. Higher-order terms of $\mathbf{u}^l(\mathbf{R}_G)$ can yield one-phonon processes. We can see this by writing $V^{G_f}_{n_f,n_i}(z)$ with the truncated V in the form

$$V^{G_f}_{n_f,n_i}(z)=\frac{N}{L^3}\sum_{l,k_z}u_{\mathbf{k}_{G_f}}e^{i(k_z z-\mathbf{k}_{G_f}\cdot\mathbf{r}_l)}(-i)\left[\frac{\hbar}{2N\omega_s(\mathbf{Q})}\right]^{1/2}\mathbf{k}_{G_f}\cdot\begin{cases}\epsilon_s^{l*}(\mathbf{Q})(n_{iQ,s}+1)^{1/2} & \text{(emission)}\\ \epsilon_s^l(\mathbf{Q})(n_{iQ,s})^{1/2} & \text{(annihilation)}\ ,\end{cases} \tag{43}$$

and comparing it with the "complete" potential matrix element given by Eq. (29), where the same n_i, n_f, and $\mathbf{G}_f$, for one-phonon transitions are substituted. The only difference between these two potential matrix elements is that the last product in Eq. (29) is absent. This product represents higher-order interactions of $\mathbf{u}^l(\mathbf{R}_G)$ in V for one-phonon transitions. The approximation made in Sec. II D on the sum over j in Eq. (27) does contain information from $\mathbf{u}^l(\mathbf{R}_G)$ of orders higher than the first. From this factor we also see that if V contains $\mathbf{u}^l(\mathbf{R}_G)$ only up to the first order, there would be no Debye-Waller factor in Eq. (31). The Debye-Waller factor results from an approximation of higher-order interactions of one-phonon processes.

III. CALCULATIONS AND RESULTS

A. Surface lattice vibration of the crystal

To obtain the dispersion relation and the polarization vectors we approximate the semi-infinite crystal by a slab of 80 layers. Since the computer time required to diagonalize the dynamical matrix increases rapidly with the number of layers and a large number of dynamical matrices needs to be diagonalized in the Debye-Waller coefficients given by Eq. (38), an 80-layer slab is a reasonable choice. For the Cu(111) surface, we choose a simple model of nearest-neighbor interaction between crystal atoms and neglect surface relaxation and reconstruction. We further assume that the pair potential is minimum when the distance between the two atoms is equal to the nearest-neighbor separation. Due to the existence of the surface, the force constant between the atoms on the two surfaces of the slab is not the same as that in the bulk. For the intralayer surface force constant k_s we adopt the value obtained by Mohamed *et al.*,[44] $k_s=0.85k_0$ where $k_0=2.49\times10^4$ dyn/cm is the bulk force constant. The phonon wave vectors under consideration vary from the $\bar{\Gamma}$ point along the $\langle 1\bar{1}0\rangle$ direction in the two-dimensional first Brillouin zone. The surface and the direction are illustrated in Fig. 2.

Since the dispersion relations are intimately related to the differential reflection coefficient of the phonon transition, we examine their behavior obtained from our model. Figure 3 shows the lowest three dispersion curves for Cu(111) from $Q=0.05$ to 0.60 Å^{-1} along the $\langle 1\bar{1}0\rangle$ direction. The lowest two dispersion curves are so close that they are nearly degenerate except near the origin. The corresponding polarization vectors $\epsilon_1^l(\mathbf{Q})$ and $\epsilon_2^l(\mathbf{Q})$ correspond to the antisymmetric and symmetric plate modes, respectively, in the continuum slab dynamics.[45] The third lowest dispersion curve lies some distance away above the first two and does not mix with them. If the number of layers is increased, it is found that the splitting of the lowest two dispersion curves decreases. For a semi-infinite crystal, the lowest dispersion curve is expected to be doubly degenerate for all $\mathbf{Q}$. For a slab of 80 layers, since the lowest two dispersion curves are nearly degenerate, their contributions to the differential reflection coefficients can be treated as additive.

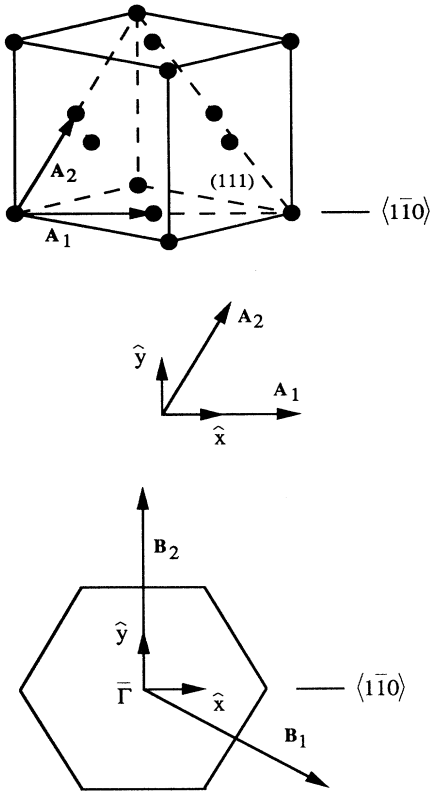

FIG. 2. Top: the fcc unit cell, the (111) surface and the ⟨1$\bar{1}$0⟩ direction. The triangle indicates the (111) surface. Middle: the coordinates on the surface. Bottom: the two-dimensional first Brillouin zone.

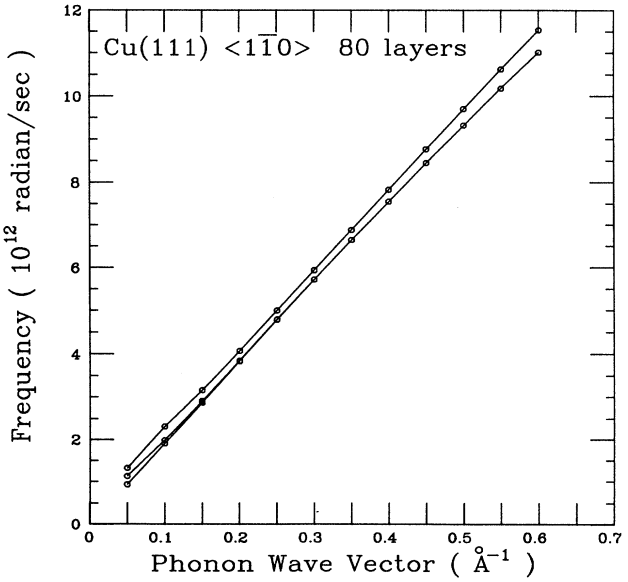

FIG. 3. The lowest three dispersion curves. The circles are calculated points.

Surface modes are characterized by the fact that the vibration amplitudes are large near the surface and decrease rapidly as the depth is increased. Experimental measurement mainly arises from the Rayleigh modes of the top side of the surface and the eigenvectors of the plate modes are to be mapped onto the Rayleigh modes by a linear transformation for the calculation of the

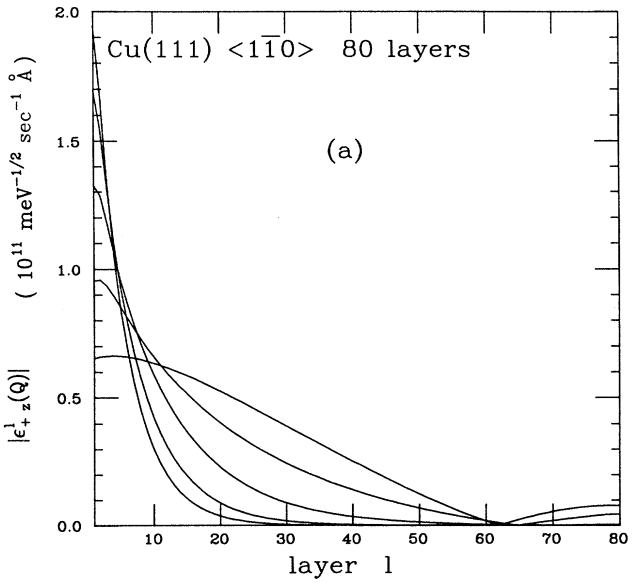

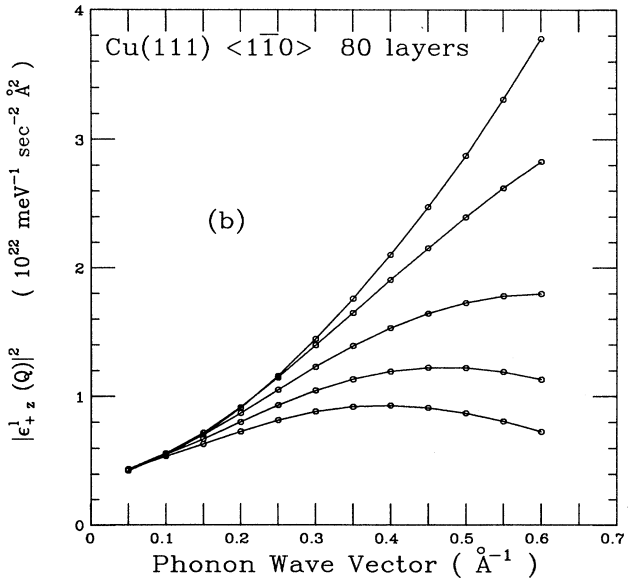

FIG. 4. (a) $|\epsilon^l_{+z}(Q)|$ against the layer l. The calculated values are connected by line segments to form curves. The curves correspond to Q=0.05, 0.20, 0.35, 0.50, and 0.60 Å^{-1} along the ⟨1$\bar{1}$0⟩ direction. $|\epsilon^l_{+z}(Q)|$ with larger Q decay faster into the slab. (b) $|\epsilon^l_{+z}(Q)|^2$ as a function of Q for the first five layers. Deeper layers correspond to smaller values at Q=0.60 Å^{-1}.

reflection coefficient. Since the lowest two modes are nearly degenerate, we define

$$\epsilon_{\pm}^{l}(\mathbf{Q}) \equiv \frac{1}{\sqrt{2}}[\epsilon_{1}^{l}(\mathbf{Q}) \pm \epsilon_{2}^{l}(\mathbf{Q})] , \tag{44}$$

where on the right-hand side the polarization vectors are normalized according to Eq. (2) and $\epsilon_{2}^{l}(\mathbf{Q})$ is multiplied by a phase factor so that the phase of the complex number $\epsilon_{2z}^{1}(\mathbf{Q})$ is the same as the phase of $\epsilon_{1z}^{1}(\mathbf{Q})$. In our case we found that for each l in the upper half slab $\epsilon_{1z}^{l}(\mathbf{Q})$ and $\epsilon_{2z}^{l}(\mathbf{Q})$ then become parallel in the complex plane and in the lower half slab antiparallel. The corresponding phonon frequencies are approximated by the averages of the lowest two frequencies. $\epsilon_{\pm}^{l}(\mathbf{Q})$ are then regarded as degenerate eigenvectors of the dynamical matrix with these phonon frequencies as eigenvalues in the region of Q where the splitting is negligible. For $Q<0.2$ Å^{-1}, which is within the range of splitting of the slab modes, this mapping is considered to be an approximation. We will refer to the phonon transition in the mapped modes by simply specifying the values of $\mathbf{Q}$. In Fig. 4(a) we plot $|\epsilon_{+z}^{l}(Q)|$ against the layer index l. We see that $|\epsilon_{+z}^{l}(Q)|$ decreases as the depth is increased. For larger Q the exponential decay is more obvious and faster. This is the Rayleigh mode for the top surface. $|\epsilon_{-z}^{l}(Q)|$ is the "mirror image" of $|\epsilon_{+z}^{l}(Q)|$ about the center plane of the slab, i.e., it is the Rayleigh mode attached to the other surface and therefore is negligible for the first few layers of the top surface.

Since the z component of the polarization vector contributes differently from the x and y components to the scattering reflection coefficient, we also plot in Fig. 4(b) $|\epsilon_{+z}^{l}(Q)|^2$ as a function of Q for the first five layers. The behavior of $|\epsilon_{+z}^{l}(Q)|^2$ on the surface is to be compared with the linear behavior obtained from the continuum model that treats the crystal as semi-infinite and is valid in the long-wavelength limit. The derivation of $|\epsilon_{+z}^{l}(Q)|^2$ from linearity is due to the finite thickness of the crystal that we took. We tested a 200-layer slab and found that $|\epsilon_{+z}^{l}(Q)|^2$ approaches linear form. We also note that the orthonormality condition is always satisfied in our discrete-lattice calculation while in the continuum model it is not considered.

B. The Debye-Waller coefficients

The sums in the expression of the Debye-Waller coefficients given by Eq. (38) are to be taken over all modes in the first Brillouin zone. It can be shown that in the harmonic approximation for the surface the eigenvalue $M_{\rm cr}\omega_s^2(\mathbf{Q})=0$ is threefold degenerate at $\bar{\Gamma}$. We believe that in a real crystal where anharmonic terms exist, $\omega_s(\mathbf{Q})$ does not decrease to zero at $\mathbf{Q}=0$. Thus we exclude the $\omega_s(\mathbf{Q})=0$ points in order to approximate a real crystal.

Through the boundary condition the number of the unit cells N determines the number of $\mathbf{Q}$ points in the first Brillouin zone and the proximity of some of these points to $\bar{\Gamma}$. Numerically these may affect the values of the Debye-Waller coefficients. We examine how to choose a reasonable length for the large primitive cell and how to carry out the summations in order to evaluate the Debye-Waller coefficients. For a microscopically large crystal with perfect two-dimensional translational symmetry, a very large number of $\mathbf{Q}$ points must be summed over. Since for small Q the value of $\omega_s(\mathbf{Q})$ may approach zero and some $\omega_s(Q)$ has the form $\omega_s(Q)=cQ+\cdots$ along a certain direction, we find the Debye-Waller coefficients diverge as $Q\rightarrow 0$. Therefore if we replace the summation over $\mathbf{Q}$ in Eq. (38) by integration, we need to know where to truncate the integral near the origin. This truncating range will be crucial; yet it is unknown. We found that for 80 layers $|\epsilon_{sz}^{l}(\mathbf{Q})|$ of the lowest three modes is not zero at the origin, and so the divergence is certain to happen. On the other hand, we found numerically that the polarization vectors, when normalized by Eq. (2), decrease as the number of layers is increased. If this number is large, the polarization vectors may be compatible with the phonon frequencies at small Q. Then the contribution of terms near the origin in the sum may not be important. In this respect, the Debye-Waller coefficients may remain some finite values which are not large even in the harmonic approximation, as long as we remove those singular points. However, the decrease in the value of the polarization vectors is too slow and the large dimension of the dynamical matrix makes the numerical calculation very difficult. Therefore we cannot replace summation by integration in evaluating the Debye-Waller coefficients.

A "perfect" real crystal is never periodic over an infinite size. The "flat" area is a few hundred angstroms in dimension. We assume a large square primitive cell on the surface with cell length equal to 50 times the nearest-neighbor distance (2.56 Å). This choice avoids using the unknown behavior of $\omega_s(\mathbf{Q})$ near $\bar{\Gamma}$. The terms in the sum in Eq. (38) are symmetrical about the origin. For the cell length chosen above, a summation over about 1440 $\mathbf{Q}$ points in half of the first Brillouin zone is calculated [i.e., the $(3\times 80)\times(3\times 80)$ dynamical matrix is diagonalized about 1440 times]. The sum is also over all modes at every $\mathbf{Q}$. Then the result is multiplied by a factor of 2 using the symmetry of $\omega_s(\mathbf{Q})$ and $\epsilon_s^l(\mathbf{Q})$ about the origin. Finally terms corresponding to $\mathbf{Q}=\mathbf{0}$ are added. Here we used much more $\mathbf{Q}$ points than usual[46] and expected to obtain a better approximation. In all the sums the $\omega_s(\mathbf{Q})=0$ modes are excluded. The Debye-Waller coefficients are symmetrical about the central plane of the slab crystal, but no more than five layers are needed for evaluating the differential reflection coefficient. The absolute values of the Debye-Waller coefficients increase by a factor of 3–4 as the temperature is raised from 60 to 300 K. This shows that the Debye-Waller factor is more important at higher temperatures. However, we found that in general these coefficients are all small $[B_{1,2}^{l}(T), C_{2}^{l}(T) \approx 10^{-6}$ and $A^{l}(T), C_{1,3}^{l}(T) \approx 10^{-3}]$. This implies that the effect of the Debye-Waller factor on the reflection coefficient is small in the temperature range 60–300 K considered here. The smallness of the coefficient $A^{l}(T)$ is worth some attention. In Eq. (40) the small $A^{l}(T)$ gives the z component of the polarization vector a heavy weight; this enhances the dominance of $\epsilon_{sz}^{l}(Q)$ over other components.

C. The interaction potentials

Based on the pair potential $u(\mathbf{r})=u(r)$ between the projectile and a crystal atom, the interaction potential between the projectiles and a rigid (static) crystal can be expanded in a two-dimensional Fourier series,

$$v(\mathbf{r})=V(\mathbf{r},\mathbf{u}^l(\mathbf{R}_G)=\mathbf{0})=\sum_{G,l}u(|\mathbf{r}-\mathbf{R}_G-\mathbf{r}_l|)$$
$$=\sum_{\mathbf{G}}v_G(z)e^{i\mathbf{G}\cdot\mathbf{R}}\ . \tag{45}$$

The Fourier components $v_G(z)$ can be expressed in terms of $u(r)$ as

$$v_G(z)=\frac{1}{S}\int_{\text{u.c.}}\left[\sum_{G',l}u(|\mathbf{r}-\mathbf{R}_{G'}-\mathbf{r}_l|)\right]e^{-i\mathbf{G}\cdot\mathbf{R}}d^2R$$
$$=\frac{1}{S}\sum_l e^{-i\mathbf{G}\cdot\mathbf{R}_l}u_G(z-r_{lz})\ , \tag{46}$$

where S is the area of the unit cell. The $u_G(z)$ can be changed to a one-dimensional integral

$$u_G(z)=2\pi\int_0^\infty dR\ u[(R^2+z^2)^{1/2}]J_0(GR)R \tag{47}$$

where $J_0(x)$ is the zeroth-order Bessel function of the first kind. In our numerical calculation we choose to use the pair interaction potential obtained by Eichenauer *et al.*[43]

D. The kinematic conditions

We describe the relations among the energies and momenta for calculating the reflection coefficient. We consider only the $\mathbf{G}_f=\mathbf{0}$ case when no diffraction takes place. In addition, we choose $k_{iz}<0$ and $k_{fz}>0$. The incident energy E_i^P is fixed so is the sum of the incident angle θ_i and the outgoing angle θ_f. The phonon wave vector $\mathbf{Q}$ and the direction of $\mathbf{K}_i$ are input variables. From Eqs. (22a) and (22b) the final energy of the projectile E_f^P is obtained to calculate K_i, which in turn is used to calculate all components of the momenta of the projectile $\mathbf{k}_{i,f}$. If $E_f^P\le 0$ or if there is no solution for K_i, no phonon transition in the mode $\mathbf{Q}$ corresponding to scattered final states $e^{i\mathbf{k}_f\cdot\mathbf{r}}|n_f\rangle$ occurs because the conservation laws and/or the scattering conditions cannot be satisfied. This procedure is used for both phonon emission and annihilation processes.

We choose the incident energy E_i^P at 9.15 meV and $\theta_i+\theta_f$ fixed at 90° to be consistent with the experimental conditions.[43] The phonon wave vector $\mathbf{Q}$ of the transition is in the opposite direction to $\mathbf{K}_i$ corresponding to in-plane scattering. Since the phonon wave vectors are input, we can select the modes of the transition. To stimulate phonon transition with Q varying from 0.05 to 0.60 Å^{-1} along the $\langle 1\bar{1}0\rangle$ direction, the incident angle θ_i increases from about 46° to 58° for phonon annihilation process and decreases from 43° to 17° for phonon emission process. The corresponding energy range of E_{iz}^P varies from 4.34 to 2.55 meV for phonon annihilation and from 4.83 to 8.37 meV for phonon emission. The corresponding values for E_{fz}^P vary from 5.17 to 11.8 meV and from 4.00 to 0.163 meV, respectively. The outgoing projectile has higher E_{fz}^P if it annihilates a phonon rather than emits one. Here E_{fz}^P is not necessarily always larger than the incident energy E_i^P even in the phonon annihilation case, since the phonon energy can be transferred to the projectile in the horizontal direction and contributes to the momentum in that direction.

E. The differential reflection coefficient

In this section, we present and analyze the calculated differential reflection coefficient based on the results of the previous sections and on Eqs. (23), (39), and (40). In our calculation, the difference of the phonon frequencies between the second and the third lowest modes is larger than the value that can usually be resolved by the conservation laws and so we do not include the differential reflection coefficient correspnding to the third lowest mode. The differential reflection coefficient with the phonon transition mode $\mathbf{Q}$ for both emission and annihilation are calculated as a function of the phonon wave vectors extending from $\bar{\Gamma}$ in the first Brillouin zone along the $\langle 1\bar{1}0\rangle$ direction, as in the case of $\omega_s(\mathbf{Q})$. Figure 5 shows the calculated differential reflection coefficient. We use the convention that negative Q represents phonon annihilation in the mode $\mathbf{Q}$ and positive Q phonon emission in the same mode. The crystal temperature is chosen at 300 K. The unit of the differential reflection coefficient is arbitrary in the sense that a constant prefactor is dropped in the calculation. On a logarithmic scale, this allows an arbitrary upward or downward translation of the curves on the graph. In the figure the upper two branches correspond to the surface modes associated with the polariza-

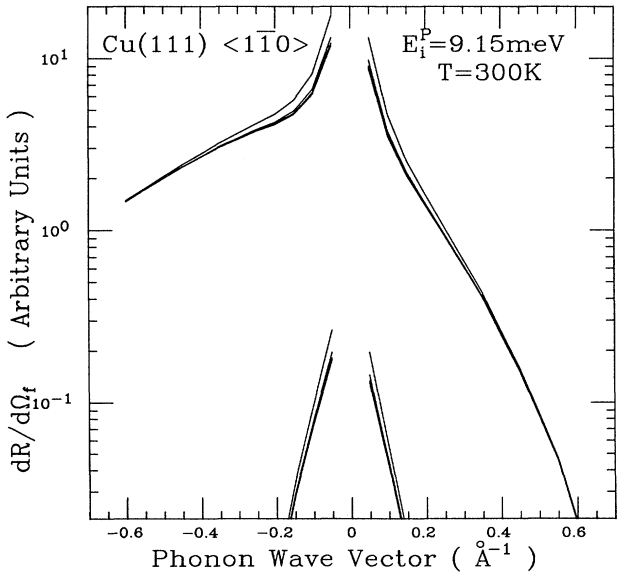

FIG. 5. The differential reflection coefficient corresponding to $\epsilon_+^l(Q)$ (the upper branches) and $\epsilon_-^l(Q)$ (the lower branches) along the $\langle 1\bar{1}0\rangle$ direction.

tion vectors $\epsilon^l_+(\mathbf{Q})$ and the lower two correspond to those associated with $\epsilon^l_-(\mathbf{Q})$. The lower branches are small compared with the upper branches and can be neglected. The curves in each branch show the differential reflection coefficient containing the sum over l in Eq. (40) down to the first, the second, . . . , the fifth layer. Thus they show different degree of perturbation due to the corrugation and the thermal motion in the first few layers. In the same figure the rigid potential $v_0(z)$ used to calculate the wave functions includes all the layers. The shape of the differential reflection coefficient is in good agreement with experiment.[43] We note that since the transformation from $\epsilon^l_1(\mathbf{Q}),\epsilon^l_2(\mathbf{Q})$ to $\epsilon^l_+(\mathbf{Q}),\epsilon^l_-(\mathbf{Q})$ is unitary as seen in Eq. (44), the reflection coefficient summed over $s=1,2$ is the same as that summed over the two Rayleigh modes. Since the lowest two dispersion curves are (nearly) degenerate, we can see from the conservation laws Eqs. (22a) and (22b) that for two modes with the same $\mathbf{Q}$, the solutions of the momenta of the projectile $\mathbf{k}_{i,f}$ are identical. We expect that from the measurement of the initial and the final energies and momenta of the projectile one cannot distinguish these two modes. The measured quantity is the totality of the corresponding differential reflection coefficients. Therefore we should add the differential reflection coefficient of the two modes and treat them as a whole. However, since $\epsilon^l_-(\mathbf{Q})$ is attached to the other surface, this summation becomes unnecessary.

We study the multiplicative factor A in the T-matrix element defined in Eq. (40). In Fig. 6(a) we plot A on a linear scale corresponding to the curves for $\epsilon^l_+(\mathbf{Q})$ in Fig. 5 against phonon wave vectors. We see that the interaction on the surface is most important. This factor decreases when the vibrational motion of the atoms in the second layer is added to that of the first. Vibrations of deeper layers do not change this summation significantly although they reduce it further. Overall the interference from the vibration of more than one layer leads to a reduction in A. This can be interpreted by the fact that the motion of the crystal atoms in deep layers in the interaction with the projectile allows more degrees of freedom to respond to the pair potential and therefore weakens the rigid interaction. For $|\mathbf{Q}|$ close to 0.60 Å^{-1} the contribution from the second and deeper layers becomes very small. Thus deeper layers contribute less and a projectile with parallel momentum transfer greater than about 0.60 Å^{-1} can barely affect the second layer.

We examine the shape of the curves in Fig. 5. For comparison we also plot A on a logarithmic scale in Fig. 6(b). The differential reflection coefficient becomes large when $|\mathbf{Q}|$ approaches the origin, since the phonon frequency approaches zero while A approaches finite values. As pointed out before, $\omega_s(\mathbf{Q})$ does not approach zero in a real crystal. Also if there is a large number of layers, the normalized polarization vectors for each layer may be small so that $|\epsilon^l_{sx,y,z}(Q)|/\omega_s(Q)$ remains finite. Thus the peak at small $|\mathbf{Q}|$ should be narrowed. The two tails of the reflection coefficient decrease faster than those of A. This is attributed to the increasing $\omega_s(Q)$ in Eq. (39) and indicates that it is more difficult to create or annihilate phonons with higher frequencies. From the Bose-Einstein distribution, lower-frequency phonons are more abundant and therefore increase the chance for transitions of long-wavelength phonons.

The Debye-Waller coefficients are small for all the temperatures so the Debye-Waller factor is expected to have a small effect on the differential reflection coefficient. To examine this, we exclude the factor $1/\{\exp[\beta\hbar\omega_s(Q)]-1\}$ from the differential reflection coefficient for the phonon annihilation branch and $1/\{\exp[\beta\hbar\omega_s(Q)]-1\}$

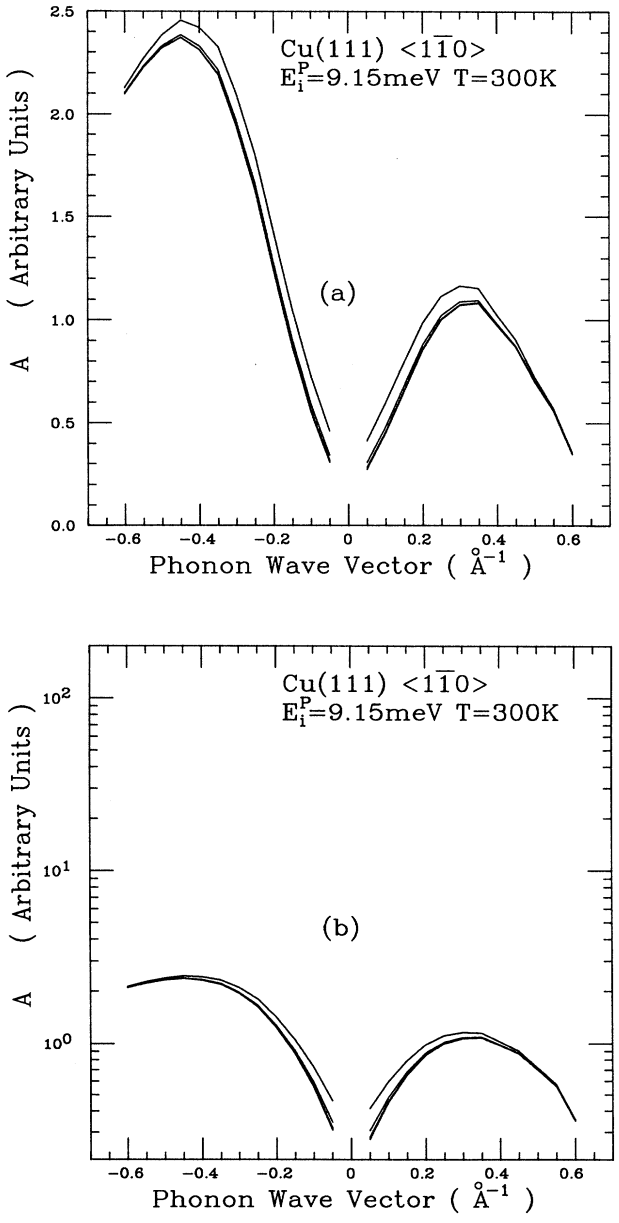

FIG. 6. (a) The factor A in Eq. (40) corresponding to the upper branches of the differential reflection coefficient in Fig. 5. (b) The factor A on the logarithmic scale.

+1 for the phonon emission branch and plot the remaining parts for temperatures between 60 and 300 K. The results are shown in Fig. 7, where the sum over the first five layers is used. We find that there is a 5%–10% increase for different Q. Since the Debye-Waller coefficients were obtained by making an approximation to the higher-order terms of the crystal-atom displacements in the interaction potential V (see the discussion in Sec. II E), this increase shows roughly how the displacements contribute to the interaction between the helium atom and the crystal as the temperature is increased.

We examine the asymmetry of the differential reflection coefficient on the two sides of the origin in Fig. 5. From Fig. 6(a) we see that A is larger for annihilation at any $|\mathbf{Q}|$ than for emission at the same $|\mathbf{Q}|$. For $\mathbf{G}_f=\mathbf{0}$ we observe the fact that the product of factors involving $\Delta\mathbf{K}$ in $\sum_l \cdots$ in Eq. (40) for phonon emission with wave vector $\mathbf{Q}$ is equal to the negative complex conjugate of that for phonon annihilation with the same $\mathbf{Q}$. Thus the difference in A between the two branches is solely due to the wave functions. We note that these wave functions are different due to the kinematic conditions. The term "+1" in "$\langle n_{i\mathbf{Q},s}\rangle_T+1$" in Eq. (39) is due to the fact that for the emission process the final phonon state has one phonon more than the initial state in the transition mode. This accounts for the emission of phonons at low temperature. To see which of the above two competing factors is stronger we plot in Fig. 8 $\langle|T_{n_f0,n_i0}|^2\rangle_T$ at 60, 140, 220, and 300 K., The sum over l is down to the fifth layer. Both branches in the figure are lowered as the temperature is decreased. This is mainly due to the Bose-Einstein distribution of the phonons. The shape of the curves remains the same as the temperature is changed. We see that the kinematic conditions are dominant at high temperatures. The annihilation curve drops faster than the emission one and this dominance is suppressed because at low temperature there are not many phonons to be annihilated. This has been experimentally observed for the system He-Cu(100) with $T=16$ K and $E_i^P=22.6$

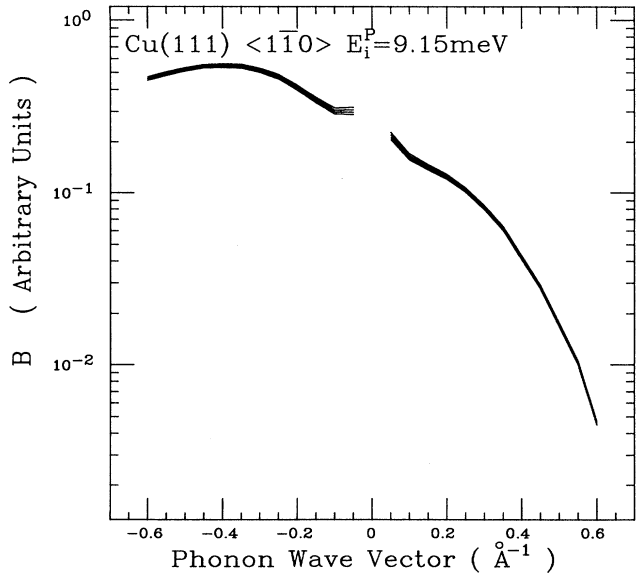

FIG. 7. $B\equiv(dR/d\Omega_f)/(1/\{\exp[\beta\hbar\omega_s(Q)]-1\}(+1))$. The term "+1" is for phonon emission. The temperatures are at 60, 140, 220, and 300 K. The higher curves correspond to higher temperatures.

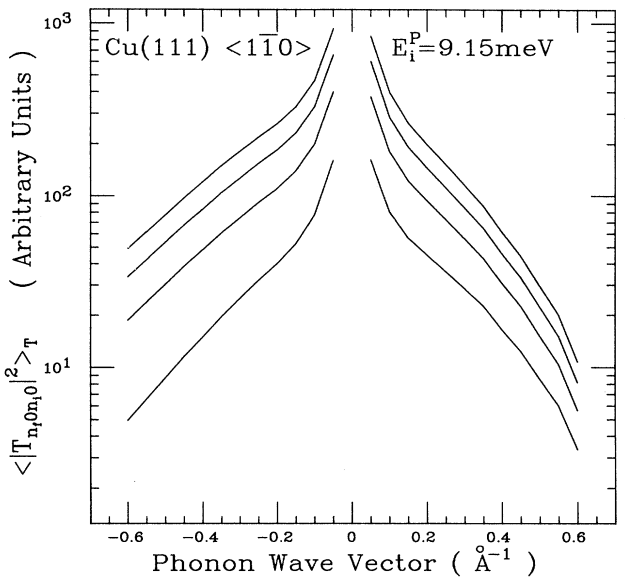

FIG. 8. $\langle|T_{n_f0n_i0}|^2\rangle_T$. The temperatures are at 60, 140, 220, and 300 K. The higher curves correspond to higher temperatures.

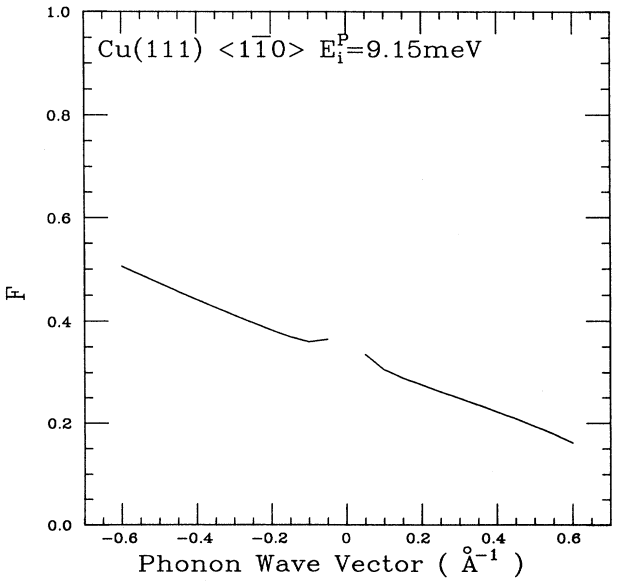

FIG. 9. The factor F.

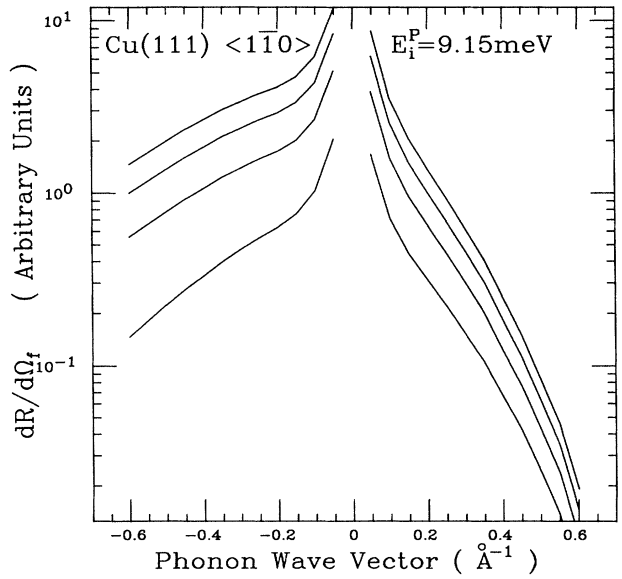

FIG. 10. The differential reflection coefficient at 60, 140, 220, and 300 K. The higher curves correspond to higher temperatures.

meV.[6] The finite values of $\langle |T_{n_f 0, n_i 0}|^2 \rangle_T$ for the emission branch at low temperature indicate that phonons can be created at any temperature regardless of how many there may be initially in thermal equilibrium.

There are other factors that affect the differential reflection coefficient. The factor $F \equiv 1/|1-\cdots|$ in Eq. (23) is due to the conservation laws. If its denominator is close to zero the differential reflection coefficient will be peaked at the corresponding **Q**. Figure 9 shows that F for phonon annihilation is always larger than that for phonon emission at the same $|\mathbf{Q}|$. The density of the final states of the outgoing atom allows more states for larger outgoing energies and therefore a larger chance for phonon annihilation. The factor $1/|k_{iz}|$ decreases as Q goes from the phonon annihilation branch to the phonon emission branch. Both factors also depend on the kinematic conditions. So the conservation laws for a given incident energy tend to annihilate phonons rather than to create them under the kinematic conditions described in Sec. III D. We note that the functions A, F, the density of the final states of the projectile, and k_{iz} are independent of the temperature. Overall the "+1" term in "$\langle n_{i\mathbf{Q},s} \rangle_T + 1$" in Eq. (39) is the only factor that favors phonon emission. In Fig. 10 we show the differential reflection coefficient at 60, 140, 220, and 300 K. Comparing with Fig. 8, we see that the phonon annihilation branch is very much enhanced by F, the density of the final states, and k_{iz}. From Fig. 10 we can infer that if the crystal is below $\sim$100 K, i.e., the temperature of a volume of helium gas with average kinetic energy equal to the incident energy of the scattering, the phonon annihilation branch would still be much higher than the phonon emission branch.

IV. SUMMARY

Based on the DWBA scheme within the T-matrix formulation, we have computed He-Cu(111) one-phonon transition reflection coefficient. This was derived from a time-independent *ab initio* scattering theory in which the interaction potential between the projectile and the crystal atoms can be an arbitrarily input and the one-phonon transition is treated more physically. With approximations the T-matrix elements for one-phonon transitions are written in a form in which we introduced the inelastic Debye-Waller coefficients to describe the thermal motion of the surface. Also we have examined the effect of truncating the atom-surface potential to first order of the displacements of the crystal atoms. We conclude that the Debye-Waller factor contains higher-order interactions. The truncation can be used as an approximation to multiphonon scattering but does not represent the complete interaction of one-phonon transitions.

We have calculated the lowest two dispersion curves and the polarization vectors of Cu(111) in the long-wavelength region ($Q \leq 0.60$ Å^{-1}) along the $\langle 1\bar{1}0 \rangle$ direction based on a model of an 80-layer slab with nearest-neighbor interaction. The force constant on the surface is taken to be 85% of that in the bulk.[44] We find the lowest two dispersion curves are nearly degenerate. The corresponding plate modes are mapped onto the Rayleigh modes employing a linear (unitary) transformation given by Eq. (44). These modes show an exponential decay behavior into the slab. The squared absolute value of the normal component of these modes is roughly linear with respect to the length of the phonon wave vector.

The Debye-Waller coefficients are calculated, assuming the length of the "large primitive cell" to be 50 times the nearest-neighbor distance. We have used discrete summation instead of continuous integration. We find the values of these coefficients increase as the temperature is raised. Their effects on the differential reflection coefficient are small as the temperature of the surface is changed.

The interaction potential between the projectile and the surface is taken to be a sum of the pair interaction. We have adopted the parameters of the He-Cu pair interaction obtained by Eichenauer *et al.*[43] The incident energy of the He atom is chosen at 9.15 meV and the surface temperature at 300 K. The scattering is in-plane and the sum of the incident and the observing angle is fixed at 90° for the purpose of comparison with experiments in Ref. 43.

We have presented the calculated results of the differential reflection coefficient of inelastic scattering of helium atoms from copper (111) surface. The one-phonon transition is in the Rayleigh modes. The shape of the differential reflection coefficient is in good agreement with experiment.[43] We find that the interaction of the projectile with the surface layer is most important. When the thermal motion of crystal atoms down to more layers is included in the interaction with the projectile, the differential reflection coefficients reduce only slightly. Further we find that the He atom with parallel momentum transfer greater than about 0.60 Å^{-1} barely affects the second layer. The peak in the differential reflection

coefficient near $Q=0$ is due to the singularity of the phonon frequency and may be narrowed if the number of layers of the slab model is increased. The decreasing tails are partly due to the increasing phonon frequencies.

We have examined the temperature dependence of the differential reflection coefficient due to the Debye-Waller coefficients. The contribution of Debye-Waller coefficients corresponds to an increase of up to 10% as T increases from 60 to 300 K.

The asymmetry of the two branches of the sum over layers for phonon emission and annihilation is solely due to the wave functions in the normal process ($\mathbf{G}_f=\mathbf{0}$). The emission process is favored by the phonon states. The kinematic conditions governing the wave functions suppress the phonon emission process at high temperatures. At low temperature, the phonon annihilation process is reduced due to the lack of phonons while the phonon emission process is always possible. The kinematic conditions, together with the density of the final states and k_{iz}, are independent of the temperature and favor phonon annihilation. Due to the Bose-Einstein distribution the differential reflection coefficient decreases if the surface temperature is lowered.

Compared to experiments, there are other contributions to the differential reflection coefficient corresponding to the lowest dispersion curve, e.g., the multiphonon transition, closed-channel effect in phonon-mediated selective adsorption and desorption, and transition in higher modes involving the bulk band. These contributions may be small in general and would involve higher-order approximations, which could be very complicated for making theoretical estimates due to the large amount of phonon channels involved. These problems are under further investigation.

ACKNOWLEDGMENTS

We would like to express our appreciation for helpful discussions with A. A. Maradudin and P. Feibelman. The allocation of computer time from San Diego Supercomputer Center for this research is gratefully acknowledged.

[1]U. Harten, A. M. Lahee, J. Peter Toennies, and Ch. Wöll, Phys. Rev. Lett. **54**, 2619 (1985).
[2]A. M. Lahee, J. P. Toennies, and Ch. Wöll, Surf. Sci. **177**, 371 (1986); A. M. Lahee, J. R. Manson, J. P. Toennies, and Ch. Wöll, Phys. Rev. Lett. **57**, 471 (1986); J. Chem. Phys. **86**, 7194 (1987).
[3]J. P Toennies, J. Vac. Sci. Technol. A **5**, 440 (1986).
[4]H.-J. Ernst, E. Hulpke, and J. P. Toennies, Phys. Rev. Lett. **58**, 1941 (1987).
[5]J. P. Toennies, J. Vac. Sci. Technol. A **2**, 1055 (1984); J. P. Toennies and Ch. Wöll, Phys. Rev. B **36**, 4475 (1987).
[6]B. F. Mason and B. R. Williams, J. Chem. Phys. **75**, 2199 (1981); Phys. Rev. Lett. **46**, 1138 (1981); B. F. Mason, K. McGreer, and B. R. Williams, Surf. Sci. **130**, 282 (1983).
[7]R. B. Doak, U. Harten, and J. Peter Toennies, Phys. Rev. Lett. **51**, 578 (1983).
[8]U. Harten, J. P. Toennies, Christof Wöll, and G. Zhang, Phys. Rev. Lett. **55**, 2308 (1985); U. Harten, J. P. Toennies, and Ch. Wöll, *ibid.* **57**, 2947 (1986); U. Harten and J. P. Toennies, Europhys. Lett. **4**, 833 (1987).
[9]R. W. Wallis, Pro. Surf. Sci. **4**, 233 (1973).
[10]R. E. Allen, G. P. Alldredge, and F. W. de Wette, Phys. Rev. B **4**, 1648 (1971); **4**, 1661 (1971); **4**, 1682 (1971).
[11]G. Benedek, Surf. Sci. **61**, 603 (1976).
[12]J. E. Black, T. S. Rahman, and D. L. Mills, Phys. Rev. B **27**, 4072 (1983).
[13]A. A. Maradudin, E. W. Montroll, G. H. Weiss, and I. P. Ipatova, *Theory of Lattice Dynamics in the Harmonic Approximation,* Suppl. 3 to *Solid State Physics* (Academic, New York, 1971).
[14]Murray S. Daw and M. I. Baskes, Phys. Rev. B **29**, 6443 (1984).
[15]J. S. Nelson, Erik C. Sowa, and Murray S. Daw, Phys. Rev. Lett. **61**, 1977 (1988).
[16]C. S. Jayanthi, H. Bilz, W. Kress, and G. Benedek, Phys. Rev. Lett. **59**, 795 (1987).
[17]V. Bortolani, G. Santoro, U. Harten, and J. P. Toennies, Surf. Sci. **148**, 82 (1984); V. Bortolani, A. Franchini, F. Nizzoli, and G. Santoro, Surf. Sci. **152**, 811 (1985).
[18]John E. Black and R. F. Wallis, Phys. Rev. B **29**, 6972 (1984).
[19]U. Harten, J. P. Toennies, and Ch. Wöll, Faraday Discuss. Chem. Soc. **80**, 137 (1985).
[20]G. Bracco, R. Tatarek, F. Tommasini, U. Linke, and M. Persson, Phys. Rev. B **36**, 2928 (1987).
[21]R. Manson and V. Celli, Surf. Sci. **24**, 495 (1971).
[22]F. O. Goodman and W. K. Tan, J. Chem. Phys. **59**, 1805 (1973).
[23]M. Lagos and L. Birstein, Surf. Sci. **51**, 469 (1975); M. Lagos, *ibid.* **65**, 124 (1977); **71**, 414 (1978).
[24]G. Benedek and G. Seriani, Jpn. Appl. Phys. Suppl. **2**, Pt. 2, 545 (1974).
[25]N. Cabrera, V. Celli, F. O. Goodman, and J. R. Manson, Surf. Sci. **19**, 67 (1970).
[26]A. Tsuchida, Surf. Sci. **14**, 375 (1969).
[27]G. Wolken, J. Chem. Phys. **58**, 3047 (1973).
[28]M. D. Stiles, J. W. Wilkins, and Mats Persson, Phys. Rev. B **34**, 4490 (1986).
[29]J. I. Kaplan and E. Drauglis, Surf. Sci. **36**, 1 (1973).
[30]H. D. Mayer, Surf. Sci. **104**, 117 (1981).
[31]L. M. Hubbard and W. H. Miller, J. Chem. Phys. **80**, 5827 (1984).
[32]H. Chow and E. D. Thompson, Surf. Sci. **82**, 1 (1979).
[33]K. L. Wolfe and J. H. Weare, Surf. Sci. **94**, 581 (1980).
[34]S. Shindo, Surf. Sci. **159**, 283 (1985).
[35]B. H. Choi and R. T. Poe, J. Chem. Phys. **83**, 1330 (1985); **83**, 1344 (1985).
[36]G. Armand and J. R. Manson, Surf. Sci. **80**, 532 (1979).
[37]J. Idiodi, V. Bortolani, A. Franchini, G. Santoro, and V. Celli, Phys. Rev. B **35**, 6029 (1986).
[38]V. Bortolani, A. Franchini, F. Nizzoli, G. Santoro, G. Benedek, and V. Celli, Surf. Sci. **128**, 249 (1983).
[39]J. R. Manson and G. Armand, Phys. Rev. Lett. **53**, 1112 (1984); Surf. Sci. **184**, 511 (1987).
[40]N. Garcia, A. A. Maradudin, and V. Celli, Philos. Mag. A **45**, 287 (1982).
[41]A. M. Marvin, V. Celli, and F. Toigo, Surf. Sci. **154**, 121 (1985).
[42]A. C. Levi and H. Suhl, Surf. Sci. **88**, 221 (1979).

[43]D. Eichenauer, U. Harten, J. P. Toennies, and V. Celli, J. Chem. Phys. **86**, 3693 (1987).
[44]Mohamed H. Mohamed, L. L. Kesmodel, Burl M. Hall, and D. L. Mills, Phys. Rev. B **37**, 2763 (1988).
[45]G. W. Farnell and E. L. Adler, *Physica Acoustics,* edited by Warren P. Mason and R. N. Thurston (Academic, New York, 1972), Vol. IX, pp. 76ff.
[46]R. E. Allen and F. W. de Wette, Phys. Rev. **179**, 873 (1969); **179**, 887 (1969).